Available online at www.sciencedirect.com
SCIENCE DIRECT®
Combustion and Flame 136 (2004) 180–190
Combustion and Flame
www.elsevier.com/locate/jnlabr/cnf

Determination of the soot absorption function and thermal accommodation coefficient using low-fluence LII in a laminar coflow ethylene diffusion flame

David R. Snelling,[a] Fengshan Liu,[a,*] Gregory J. Smallwood,[a] and Ömer L. Gülder [b]

[a] *Combustion Technology Group, National Research Council Canada, Building M-9, 1200 Montreal Road, Ottawa, ON K1A 0R6, Canada*

[b] *University of Toronto, Institute for Aerospace Studies, 4925 Dufferin Street, Toronto, ON M3H 5T6, Canada*

Received 17 March 2003; received in revised form 1 September 2003; accepted 1 September 2003

Abstract

Effective temperatures of pulsed-laser-heated soot particles were derived from their thermal emission intensities using optical pyrometry in a laminar ethylene coflow diffusion flame. The present study concerns conditions of relatively low laser fluences under which soot particles are heated to temperatures below 3500 K to avoid complications of soot particle vaporization in both the experiment and the numerical calculations. The current nanoscale heat transfer model for laser-induced incandescence (LII) of soot was improved to account for the effect of the fractal structure of soot aggregates on the rate of heat loss to the surrounding gas. Mean primary soot particle diameter and mean aggregate size at the location of measurement were determined using the technique of thermophoretic sampling/transmission electron microscopy analysis. Numerical calculations based on the improved LII model were conducted to predict the soot particle temperature with known gas temperature, the heat conduction coefficient, the primary particle diameter, and the mean aggregate size, as well as values of assumed soot absorption function $E(m)$ and the thermal accommodation coefficient of soot α. The experimentally observed soot temperature history, characterized by the peak value and the temporal decay rate, cannot be reproduced numerically using the values of $E(m)$ and α found in the literature. By utilizing the experimental peak temperature and temporal decay rate new values of $E(m)$ at 1064 nm and α were determined. Uncertainties in the derived values of $E(m)$ and α caused by the uncertainty in the primary soot particle diameter and the mean aggregate size were analyzed. A novel method to determine the values of the soot absorption function $E(m)$ and the thermal accommodation coefficient α was developed in the present study.

Keywords: Laser diagnostics; Soot

1. Introduction

Nonintrusive optical diagnostic techniques play an important role in our understanding of soot formation, growth, and oxidation in flames. While traditional techniques can provide information on soot characteristics, including soot volume fraction by laser extinction [1] and soot morphology (primary particle diameter and aggregate size), by laser scattering [1] and thermophoretic sampling/transmission electron microscopy analysis (TS/TEM) [2], they suffer various limitations compared to the more recently developed

* Corresponding author.
E-mail address: fengshan.liu@nrc-cnrc.gc.ca (F. Liu).

0010-2180/$ – see front matter
doi:10.1016/j.combustflame.2003.09.013

laser-induced incandescence (LII) technique [3–9]. LII has been proven to be a useful diagnostic tool for spatially and temporally resolved measurement of soot volume fraction and primary particle size in a wide range of applications.

A practical method to measure the surface temperature of particles (soot, coal, and carbon) is optical pyrometry, based on the particle thermal emission intensities detected at two or more wavelengths [10–13]. When the temperature of soot particles in the measurement volume is nonuniform, the measured temperature is an *effective temperature* and is close to the peak value within the probe volume [14] or within the soot layer surrounding the parent fuel particle [13]. Various optical pyrometers have also been used to monitor the soot particle temperature during LII. Eckbreth [15] measured the laser-irradiated soot particle surface temperatures using the LII signals detected at two different wavelengths. Snelling et al. [16] employed a three-wavelength pyrometer to measure the laser-heated soot particle surface temperatures in a diesel engine exhaust. The primary soot particle diameter was also inferred from the measured temperature decay rate using an assumed value of the soot thermal accommodation coefficient.

A theoretical model describing the nanoscale heat and mass transfer processes of LII has been developed and improved over the past 2 decades [9,15,17–20]. However, significant uncertainty may still exist in the numerical results under conditions of significant soot evaporation primarily due to the lack of reliable physical parameters in the soot evaporation submodel, such as the vapor pressure and the heat of vaporization [21]. To avoid the uncertainty in the evaporation submodel, the present study focused on low laser fluence, so that the maximum soot particle temperature remains below 3500 K, ensuring negligible soot evaporation. Uncertainties also exist in the laser energy absorption and heat conduction submodels in which the refractive index (m)-dependent soot absorption function $E(m)$ and the thermal accommodation coefficient α are required to calculate the rate of laser energy absorption by soot particles and heat transfer rate between soot particles and the surrounding gas, respectively. Significant uncertainties exist in the values of the absorption function $E(m)$ of soot in the visible and near infrared, varying from about 0.2 up to about 0.4 [22]. The thermal accommodation coefficient of soot is subject to even greater uncertainty in the literature of LII modeling, from a low value of 0.26 [9] to a high value of 0.9 [18]. An accurate thermal accommodation coefficient for soot/surrounding gas is essential in the determination of the primary soot particle diameter since the calculated primary particle diameter based on the temperature decay rate is proportional to the accommodation coefficient [16].

In this study, the three-wavelength optical pyrometer employed previously by Snelling et al. [16] was used to experimentally measure the laser-heated soot particle temperatures in a coflow ethylene diffusion flame. Numerical calculations were also conducted to simulate the LII experiment using an improved LII model. The objectives of the present study were (i) to improve the current LII model by taking into account the shielding effect of heat conduction between aggregated soot particles and the surrounding gas and (ii) to develop a novel method of independently deriving the values of soot absorption function $E(m)$ at the laser wavelength and the thermal accommodation coefficient α by utilizing the experimental peak particle temperature and the temporal decay rate.

2. Experimental methods

2.1. Experimental setup

The LII experimental setup has been described in our previous study [16]. A pulsed Nd:YAG laser, operating with 60 mJ/pulse at 20 Hz and 1064 nm, was used as the excitation source. A half-wave plate (to rotate the plane of polarization) in combination with a thin film polarizer (angle-tuned to transmit horizontally polarized radiation) was used to control the laser energy per pulse. The beam was then focused with a cylindrical lens to form a sheet through the probe volume. The beam intensity profiles in the probe volume were measured with a Coherent BeamView system. The LII signal from the center of the laser sheet was imaged onto three photomultipliers equipped with narrow-band interference filters centered at 397 nm (36 nm FWHM), 501 nm (18 nm FWHM), and 782 nm (19 nm FWHM), respectively. Transient signals from the photomultipliers were digitized and transferred to a computer for further analysis. Multipulse averages were acquired with 400 samples per average.

The burner for generating the laminar coflow ethylene diffusion flame at atmospheric pressure used in the present study has been previously described in detail in Refs. [23,24]. Briefly, the burner consists of a central fuel tube with a 10.9-mm inner diameter surrounded by an annular air nozzle of 100-mm inner diameter. The ethylene flow rate was 3.23 cm^3/s and the air flow rate was 4733 cm^3/s, resulting in a visible flame height of about 64 mm. The present LII experiments were carried out at a location 42 mm above the burner exit, on the burner centerline.

Soot morphology at the location of LII measurement in the laminar ethylene diffusion flame was determined in the present study using the technique of TS/TEM, similar to that employed previously by

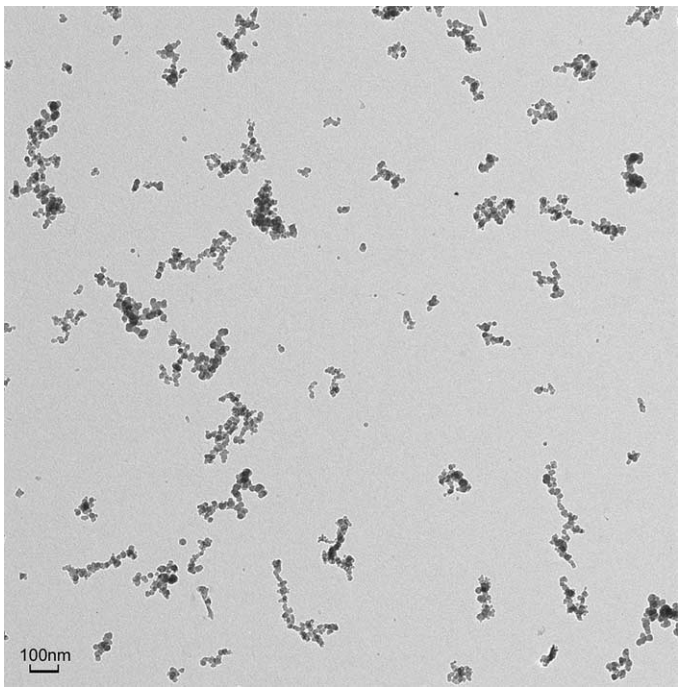

Fig. 1. A typical TEM photograph of soot sampled at the location of LII measurement.

Köylü et al. [25]. A typical TEM photograph of soot sampled at 42 mm above the burner exit on the flame centerline is shown in Fig. 1. Our own unpublished results based on TS/TEM analyses indicated that the mean primary soot particle diameter d_p and the mean aggregate size (mean number of primary soot particles per aggregate) N_p at the location of LII measurement are respectively 29 nm and 42.

2.2. Optical pyrometry

Assuming the fluence distribution across the laser beam profile is uniform, all the particles in the laser volume are heated to the same temperature. The incandescence signal detected by the system at a wavelength λ_i can be written as

$$I_i = C\frac{2\pi c^2 h}{\lambda_i^5}\left[\exp\left(\frac{hc}{\lambda_i \kappa T}\right) - 1\right]^{-1}\frac{\pi^2 d_p^3 E(m_i)}{\lambda_i}, \tag{1}$$

where C is a wavelength-independent factor of the system and the measurement location. Symbols h, c, and κ represent respectively the Planck constant, the speed of light, and the Boltzmann constant. $E(m)$ is a function of the refractive index m [20], which is wavelength dependent, hereafter referred to as the absorption function of soot. Quantity d_p represents the primary particle diameter. Subscript i is the wavelength index. At 42 mm above the burner exit in the flame investigated, the annular structure of soot merges to form a solid body structure. Consequently, the attenuation of LII signal by soot absorption in the detection path across half of the flame is expected to be small. Nevertheless, attenuation was accounted for in the experiment by measuring the laser intensity attenuation at the detection wavelengths across the flame at this height. Our experimental measurement showed that the intensity attenuation across half of the flame at 42 mm above the burner exit is less than 5% at all three detection wavelengths. Under the conditions of the present study, the exponential term in Eq. (1) is much greater than 1, therefore, Eq. (1) can also be written as

$$\frac{hc}{\kappa T}\frac{1}{\lambda_i} = \ln\left(\frac{E(m_i)}{I_i \lambda_i^6}\right) + \text{const.} \tag{2}$$

Equation (2) implies that the quantity $\ln[E(m_i)/I_i\lambda_i^6]$ detected at two or more different wavelengths should be linear with $1/\lambda_i$. The particle temperature T can then be calculated from the slope of this straight line. In practice, however, due to typical nonuniform laser beam profiles or nonuniform primary particle sizes, the soot particles in the laser volume are not uniform in temperature. The optical pyrometer derives an *effective soot particle temperature*, which is close to the highest particle temperature in the laser volume, as the signal is substantially greater for the highest temperatures. It is also important to point out that the experimentally determined soot particle temperature based on Eq. (2) depends on how $E(m)$ varies

with wavelength. To illustrate the effect of $E(m) \sim \lambda$ on the experimentally determined soot temperature, Eq. (2) is rewritten in the following form, for a two-color optical pyrometer,

$$T = \frac{hc}{\kappa} \frac{1/\lambda_1 - 1/\lambda_2}{\ln[E(m_1)/E(m_2)] + \ln(I_2\lambda_2^6/I_1\lambda_1^6)}. \quad (3)$$

Equation (3) shows that the experimentally determined soot temperature is independent of $E(m)$ if $E(m)$ is assumed to be constant at the detection wavelengths in the visible and near infrared as suggested in a recent experiment study by Snelling et al. [26]. Under this assumption, a prior knowledge of the value of $E(m)$ is not required to determine the soot particle temperature using Eq. (2) or Eq. (3). On the other hand, it is also feasible to assume that $E(m)$ increases linearly with wavelength in the visible and near infrared based on the experimental studies of Krishnan et al. [22] and Snelling et al. [26]. In the visible and near infrared (between 400 and 1064 nm), the experimental data for $E(m)$ of Krishnan et al. [22] can be fit to a linear expression, $E(m) = 0.232 + 1.2546 \times 10^{-4} \times \lambda$, where λ is in nanometers. It is worth pointing out that both possibilities were within the experimental error in the study of Snelling et al. [26]. In this case the experimentally determined soot temperature is weakly dependent on the values of $E(m)$ at the detection wavelengths, since it is the relative values of $E(m)$ at the two detection wavelengths, rather than the absolute values, that are required. As a result, a good knowledge of the absolute values of $E(m)$ at the detection wavelengths is not a prerequisite for the determination of soot particle temperature using the optical pyrometer. Both the constant $E(m)$ suggestion of Snelling et al. [26] and the linear $E(m) \sim \lambda$ relation of Krishnan et al. [22] are employed to derive the experimental soot temperatures and the results are compared.

3. Theory

3.1. Low-fluence LII model

It is well known that soot particles in flames form fractal-like structures (aggregates) with some bridging between the primary particles [2,27,28]. However, it is a reasonable approximation to model soot aggregates as monodisperse spherical primary particles that are just in point contact [28]. Although the size of primary soot particles at a given location in laminar diffusion flames has a very narrow distribution, the number of primary soot particles per aggregate has a much wider distribution [28]. A detailed consideration of the additional effect of aggregate size distribution on the cooling rate of soot aggregates in the LII measurement volume is beyond the scope of this study. A simplified treatment is to consider only the mean aggregate size (the mean number of primary particles per aggregate) as a first approximation. Considering the energy balance for soot, it is more realistic to base it upon an aggregate, compared to LII models for a single primary particle that have frequently been used in the literature [8,9,20]. Based on results from RDG-PFA theory [28], the laser heating term for primary particles is not affected by aggregation. The LII model described in Ref. [20] was modified to account for the fractal structure of soot aggregates in the calculation of heat conduction rate between a soot aggregate and the surrounding gas. In the absence of soot evaporation the energy conservation equation of a soot aggregate can be written as

$$C_a F_0 q(t) N_p - \frac{2k_a(T - T_g)\pi D_a^2}{(D_a + G\lambda_{MFP})} - \frac{1}{6}\pi d_p^3 N_p \rho_s c_s \frac{dT}{dt} = 0. \quad (4)$$

In Eq. (4), $C_a = \pi^2 d_p^3 E(m)/\lambda$ is the absorption cross section of a primary soot particle in the Rayleigh limit [20], which is proportional to $E(m)$. Thus, it is $E(m)$, and not the refractive index m, which must be known to model laser heating of the soot particles. F_0 is the laser fluence in mJ/mm^2. Function $q(t)$ is the pulsed laser temporal power density per mJ/mm^2 laser fluence. Symbols N_p, λ_{MFP}, k_a, and T_g respectively stand for the mean aggregate size (mean number of primary particles per aggregate), the mean free path of the surrounding gas, the heat conduction coefficient of the surrounding gas, and the local gas temperature. Variable G is the geometry-dependent factor [18] and is related to the Eucken factor f [29], the thermal accommodation coefficient α, and the ratio of specific heats γ of the surrounding gas through $G = 8f/\alpha(\gamma + 1)$. The mean free path λ_{MFP} is calculated using the expression given in [30] with air properties assumed for the specific heat at constant volume, the ratio of the specific heats γ, and the mean molecular weight of the surrounding gas. The diameter D_a is the diameter of an equivalent single solid sphere that has the same energy transfer surface area as the aggregate. The effective heat transfer cross section of the equivalent sphere is taken to be the projected area of an aggregate, i.e., $\pi D_a^2/4 = A_a$. This assumption seems appropriate in the free-molecular regime in which there are no intermolecular collisions over a length scale corresponding to the typical aggregate. Using a fractal description, the projected area of an aggregate is related to the number of primary particles in the aggregate and the primary particle diameter

in the following equation [31]

$$A_a = \left(\frac{N_p}{f_a}\right)^{1/\varepsilon_a} \frac{1}{4}\pi d_p^2, \tag{5}$$

where f_a and ε_a are pre factor and exponent, respectively. Using numerically generated aggregates, Brasil et al. [31] found that $\varepsilon_a = 1.08$ and $f_a = 1.10$. On the other hand, Köylü et al. [32] found that $\varepsilon_a = 1.10$ and $f_a = 1.16$ from numerical simulation and $\varepsilon_a = 1.09$ and $f_a = 1.15$ from measurements of soot in C_2H_2, C_2H_4, C_2H_6, and C_3H_8 flames under both laminar and turbulent conditions. Using Eq. (5), D_a is related to d_p and N_p through

$$D_a = \left(\frac{N_p}{f_a}\right)^{1/2\varepsilon_a} d_p. \tag{6}$$

This assumption is supported by the work of Filippov et al. [33], who calculated a scaling law for the effective cooling rate diameter in the free-molecular regime using calculated heat transfer rates for individual numerically generated aggregates. Using the scaling law of Filippov et al. [33] for complete accommodation ($\alpha = 1$), the effective diameter D_a is calculated as $D_a = d_p(N_p/k_h)^{1/D_h}$ with scaling exponent $D_h = 2.2$ and scaling pre factor $k_h = 1.2$ in the free-molecular regime. At this point it is worth pointing out that the numerical results of Filippov et al. shown in Ref. [33, Fig. 11] for the ratio of heat transfer rates between aggregated and nonaggregated particles in the free-molecular regime are questionable, since there is no physical ground for the dependence of this ratio on the thermal accommodation coefficient α. A detailed discussion of this topic is beyond the scope of the present study and will be presented in a future study. To illustrate the difference in the cooling area between the aggregate models and the single primary particle model, the ratio of the cooling areas ($\pi D_a^2/N_p\pi d_p^2$) is plotted in Fig. 2 as a function of the aggregate size. As expected, the cooling area of an aggregate is less than the total surface area of primary particles within it due to the shielding effect [34]. For typical mean aggregate sizes of 42 found at the location of the present LII measurement and 100 found near the midheight on the centerline of a coflow laminar diffusion flame [25], the aggregate cooling area is about 68 to 56% of the total surface area of individual primary particles based on Eq. (6) with the parameters of Brasil et al. [31] and the scaling law of Filippov et al. [33] given above. Moreover, the aggregate cooling area becomes less dependent on the aggregate size for N_p greater than about 50.

3.2. Theoretical effective particle temperature

It should be pointed out that the solution of Eq. (4) corresponds to a uniform laser fluence profile across the laser beam. For a nonuniform laser fluence profile, which is almost always the case in practice, proper treatment is necessary to account for the different contributions from different parts of the laser beam, where particles are heated to different temperatures, to the total emission. Once the soot particle temperatures for a range of laser fluences are obtained by solving Eq. (4), the LII signals detected at different wavelengths in the visible and near infrared can be simulated by integrating the thermal emission intensity of soot particles across the measured profile of the laser beam. The temporal and spatial distributions of the laser beam corresponding respectively to 1 mJ/mm^2 and 1 mJ for the laser used in the present experimental and numerical study are shown in Fig. 3.

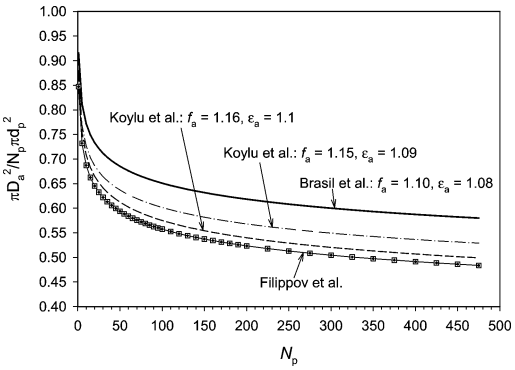

Fig. 2. Variation of $\pi D_a^2/N_p\pi d_p^2$ with the aggregate size calculated using two models: (1) based on the projected area given in Eq. (5) and (2) using the scaling law of Filippov et al. [33].

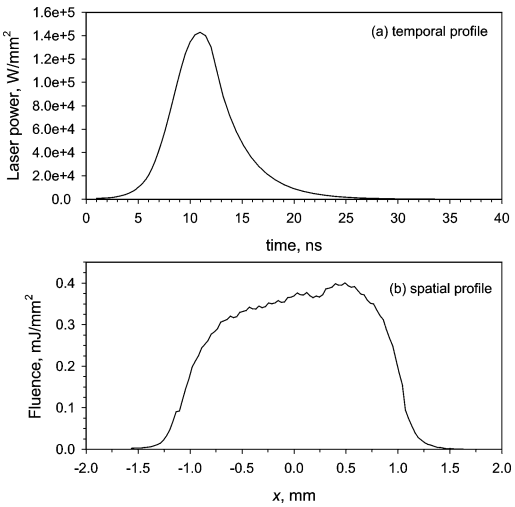

Fig. 3. Temporal and spatial distributions of the pulsed laser used in the experiment and calculations.

The spatial distribution of the laser fluence is calculated by averaging the fluence over the cross section of the laser sheet imaged by the detectors. Assuming soot particles are uniformly distributed inside the probe volume and the probe volume is small enough to ensure the optically thin assumption is valid, the total thermal emission intensity (TEI) at a wavelength λ_i can be calculated by dividing the laser beam profile into K uniform segments,

$$TEI_i = A\sum_{k=1}^{K} N\frac{2\pi c^2 h}{\lambda_i^5}\left[\exp\left(\frac{hc}{\lambda_i \kappa T_k}\right)-1\right]^{-1} \times \frac{\pi^2 d_p^3 E(m_i)}{\lambda_i}\Delta x, \quad (7)$$

where A is the cross section area of the laser volume and N is the number of primary soot particles inside each segment of width Δx; the soot particle temperature inside kth segment T_k corresponds to the solution of Eq. (4) obtained at a laser fluence of $E_0 F(x_k)$ with E_0 being the laser pulse energy in millijoules. A series of solutions at different laser energies was first obtained, then the soot particle temperature at the kth segment was calculated by linear interpolation between the solutions of its two neighboring laser fluences in the numerical calculations.

The theoretical effective particle temperature T_e is defined such that it satisfies the expression

$$\frac{TEI_1}{TEI_2} = \frac{E(m_1)}{\lambda_1^6}\frac{\lambda_2^6}{E(m_2)}\frac{\exp(hc/\kappa\lambda_2 T_e)-1}{\exp(hc/\kappa\lambda_1 T_e)-1}, \quad (8)$$

which is effectively the principle of the two-wavelength optical pyrometer. Substitution of Eq. (7) into Eq. (8) and using the approximation $\exp(hc/\kappa\lambda T) \gg 1$ leads to

$$T_e = \frac{hc}{\kappa}\left(\frac{1}{\lambda_2}-\frac{1}{\lambda_1}\right)\Big/\ln\frac{\sum_{k=1}^{K}\exp(-\frac{hc}{\kappa\lambda_1 T_k})}{\sum_{k=1}^{K}\exp(-\frac{hc}{\kappa\lambda_2 T_k})}. \quad (9)$$

Unlike the experimentally derived particle effective temperature given in Eq. (2) or Eq. (3), the theoretical effective particle temperature, Eq. (9), is independent of the absorption function $E(m)$ regardless of the functional dependence of $E(m)$ on λ. It can also be observed from Eq. (9) that the effective particle temperature derived from the ratio of thermal emission intensities at two wavelengths λ_1 and λ_2 in general depends on the values of the two wavelengths for a nonuniform laser fluence profile. The effective particle temperature is independent of wavelength if the soot particles in the laser volume are uniform in temperature, i.e., for a uniform laser fluence profile. Eq. (9) also implies that the effective particle temperature approximates the highest soot particle temperature in the laser volume as the summation of the exponential function is dominated by terms with highest temperatures.

3.3. Effects of d_p and N_p on theoretical soot particle temperature

It is of importance to investigate theoretically the effects of d_p and N_p on the calculated soot particle temperature using the LII model described above, since the measured d_p and N_p are subject to certain errors. Such theoretical analysis provides insights into how the uncertainty in d_p and N_p affects the accuracy of the derived values of $E(m)$ and α. The effects of d_p and N_p on the peak soot temperature are first analyzed. It is anticipated that the peak soot temperature occurs at a time τ_{max} near the end of the laser pulse when the heat loss rate starts to dominate the laser energy absorption rate. For $t < \tau_{max}$, the heat loss rate is negligible compared to other terms in Eq. (4). Then substitution of C_a into Eq. (4) leads to

$$\frac{dT}{dt} \approx \frac{6\pi E(m) F_0 q(t)}{\lambda \rho_s c_s}. \quad (10)$$

Integration of Eq. (10) over 0 to τ_{max} leads to

$$T_{max} \approx T_g + \frac{6\pi E(m) F_0}{\lambda \rho_s c_s}\int_0^{\tau_{max}} q(t)\,dt. \quad (11)$$

Equation (11) indicates that the peak soot temperature is nearly independent of d_p and N_p, but strongly dependent on soot properties $E(m)$, ρ_s, and c_s and the laser properties λ, F_0, and $q(t)$. Therefore knowledge of d_p and N_p, to a large extent, is not required to calculate the peak soot temperature. A quantitative effect of the heat loss term on the calculated peak soot temperature will be given later in the presentation of numerical results.

The effects of d_p and N_p on the temporal decay rate of soot temperature can be analyzed as follows. After the laser pulse, the soot temperature decay rate is entirely controlled by the heat loss rate of soot aggregates to the surrounding rate. Equation (4) can then be written as, after substitution of D_a and G and making use of the fact that $G\lambda_{MFP}$ is much greater than D_a under the conditions of this study,

$$\frac{d\ln(T-T_g)}{dt} = -\frac{3k_a\alpha(\gamma+1)}{2f\lambda_{MFP}\rho_s c_s d_p N_p}\left(\frac{N_p}{f_a}\right)^{1/\varepsilon_a}. \quad (12)$$

Equation (12) shows that the temporal decay rate of soot temperature is inversely proportional to the primary soot particle size d_p and proportional to N_p to the power of $(1/\varepsilon_a - 1)$. Since ε_a is typically about 1.1, the temporal decay rate of soot temperature is very weakly dependent on the aggregate size N_p, i.e., some uncertainty in N_p has negligible effect on the

temporal decay rate of soot temperature. However, uncertainty in d_p has significant effect on the temporal decay rate. Once the temporal decay rate, left side of Eq. (12), is determined experimentally, Eq. (12) can be used for different purposes. For example, it can be used to derive the primary soot particle size d_p if other quantities, in particular N_p and α, are considered *known*. In this study, Eq. (12) was employed to derive the value of α since all other quantities, including d_p and N_p, are known.

4. Results and discussion

The primary soot particle size and the mean aggregate size at the location of measurement (42 mm above the burner exit surface and on the centerline) were required as input parameters to the LII model to calculate the temperature history of the primary soot particles. They were also required to derive the values of $E(m)$ and α theoretically from Eqs. (11) and (12) in the case in which the peak soot temperature and temporal decay rate were determined experimentally. As mentioned earlier, these quantities were found from our TS/TEM analyses to be $d_p = 29$ nm and $N_p = 42$. Nevertheless, numerical calculations were conducted to investigate the effects of the uncertainty in d_p and N_p on the calculated soot temperature as well as the derived values of $E(m)$ and α based on the experimental peak soot temperature and the temporal decay rate. The gas temperature at the location of measurement T_g was found to be about 1700 K from our CARS measurements [24]. The heat conduction coefficient of the gas mixture at the location of LII measurement was obtained from detailed numerical modeling [35] with $k_a = 0.11$ J/m s K. The soot density and specific heat used in the present calculations are $\rho_s = 1.9$ g/cm^3 and $c_s = 2100$ J/kg K. The mean free path λ_{MFP} was found to be 603 nm. The specific heat ratio γ of the surrounding gas (approximated as that of air) and the Eucken factor f at 1700 K were found to be 1.291 and 1.656, respectively. These thermal input parameters used in the calculations are summarized in Table 1.

Solutions to Eq. (4) were obtained for a range of fluences between 0 and 2.9 mJ/mm^2 at an increment of 0.1 mJ/mm^2 and for different values of d_p, N_p, $E(m)$, and α. The theoretical effective particle temperatures were then calculated using wavelengths of 400 and 800 nm in Eq. (9). The degree of agreement between the numerical soot temperature history, characterized by the peak temperature and the temporal decay rate, based on values of $E(m)$ and α found in the literature and experimentally provides a direct test of the accuracy of these values. Likewise, the experimental soot temperature history can be used to derive the values of $E(m)$ and α using Eqs. (11) and (12).

Table 1
Thermal parameters at 42 mm above the burner exit on the flame centerline

Thermal parameter	Value
Gas temperature T_g	1700 K
Heat conduction coefficient k_a	0.11 J/m s K
Soot density ρ_s	1.9 g/cm^3
Specific heat of soot c_s	2100 J/kg K
Mean free path λ_{MFP}	603 nm
Specific heat ratio γ	1.291
Eucken factor f	1.656

4.1. Sensitivity of calculated particle temperature to $E(m)$, α, d_p, and N_p

As mentioned earlier significant uncertainties exist in the values of $E(m)$ and α. In this study, the values of $E(m)$ and α were determined independently by matching the theoretical effective particle temperatures (peak value and temporal decay rate) to those derived experimentally. To understand how this task can be accomplished, it is important to appreciate the different roles of $E(m)$ and α in the calculation of the theoretical effective particle temperatures. Unless otherwise indicated, a uniform laser profile with a fluence of 0.9 mJ/mm^2, $d_p = 29$ nm, $N_p = 42$, and the values of pre factor and exponent in Eq. (5) from Brasil et al. [31] were used in the following sensitivity analysis to investigate the effects of $E(m)$, α, d_p, and N_p on the calculated peak particle temperature and temporal decay rate.

Temperature histories calculated for different values of $E(m)$ (at 1064 nm) are displayed in Fig. 4 while keeping $\alpha = 0.26$. To demonstrate the sensitivity of the calculated particle temperature history to the aggregate cooling area, results based on the pre factor and exponent of Köylü et al. [32] in Eq. (5), the lower curve in Fig. 1 with $f_a = 1.16$ and $\varepsilon_a = 1.1$, are also shown in Fig. 4. The smallest value of $E(m)$ considered, 0.296, is the most commonly used one according to Dalzell and Sarofim [36]. The value of 0.366 is from a recent experimental study by Krishnan et al. [22]. The largest value considered, 0.42, demonstrates the effect of a 15% increase over the value of Krishnan et al. [22]. It can be seen that the predicted peak particle temperature is very sensitive to the value of $E(m)$ (Fig. 4a), in agreement with the theoretical analysis that the temperature rise, $T_{max} - T_g$, is proportional to $E(m)$ (Eq. (11)). Use of different values of f_a and ε_a in the aggregate projected area expression only slightly affects the temporal decay rate and has negligible effect on the peak temperature, consistent with the theoretical results shown in Eqs. (11) and

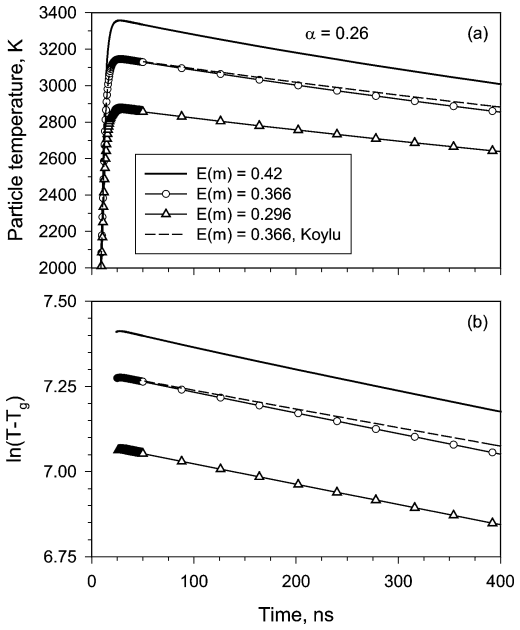

Fig. 4. Effects of $E(m)$ and the pre factor and exponent in Eq. (5) on the soot particle temperature and its decay rate calculated by the LII model at a uniform laser profile with a fluence of 0.9 mJ/mm^2 and $\alpha = 0.26$. Unless otherwise indicated, $d_p = 29$ nm, $N_p = 42$, and the pre factor and exponent in Eq. (5) from Brasil et al. [31] are used. When the pre factor and exponent in Eq. (5) from Köylü et al. [32] are used, $f_a = 1.16$ and $\alpha_a = 1.1$.

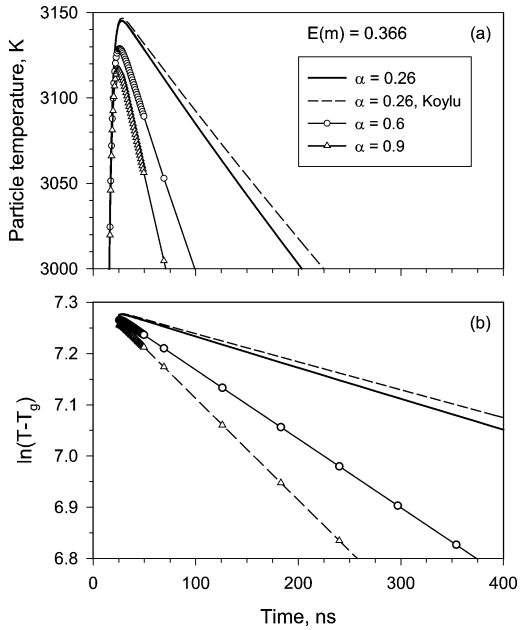

Fig. 5. Effects of the thermal accommodation coefficient on the calculated peak soot temperature and temporal decay rate at a uniform laser profile with a fluence of 0.9 mJ/mm^2 and $E(m) = 0.366$. Unless otherwise indicated, $d_p = 29$ nm, $N_p = 42$, and the pre factor and exponent in Eq. (5) from Brasil et al. [31] are used. When the pre factor and exponent in Eq. (5) from Köylü et al. [32] are used, $f_a = 1.16$ and $\alpha_a = 1.1$.

(12). Under the conditions of Fig. 4, the slope of temporal decay rate based on $f_a = 1.16$ and $\varepsilon_a = 1.1$ of Köylü et al. [32] differs from that based on values of Brasil et al. [31] by about 10%.

Figure 5 shows the calculated soot temperatures for different values of α while keeping other input parameters constant. The range of α selected covers the smallest value of 0.26 [9] and the largest one, 0.9 [18], found in the literature as well as an intermediate value of 0.6. The predicted peak soot particle temperature is only slightly affected by the value of α, the peak soot temperature decreases by only about 28 K when the value of α varies from 0.26 to 0.9 (Fig. 5a). However, the slope of the $\ln(T - T_g)$ curve (Fig. 5b) is very sensitive to the value of α since it is proportional to α as indicated by the theoretical analysis given in Eq. (12).

To demonstrate the effect of uncertainty in d_p on the calculated soot particle temperature history, numerical calculations were conducted for five different values of d_p: the measured mean diameter of 29 nm; the measured value with 10% error, 31.9 and 26.4 nm; and the measured value with 20% error, 34.8 and 24.2 nm. These results are compared in Fig. 6 for $E(m) = 0.366$ and $\alpha = 0.26$. The peak particle temperature reduces by only about 5 K when d_p varies from the maximum value, 34.8 nm, to the minimum value, 24.2 nm, considered (Fig. 6a). Thus even 20% uncertainty in d_p has a negligible effect on the calculated peak particle temperature, which is expected based on the theoretical analysis given in Eq. (11) that the soot particle temperature history before the peak value is nearly independent of the primary particle size d_p, since both the laser energy absorption and the particle internal energy change are volumetric processes and the effect of d_p is therefore canceled out. However, the uncertainty in d_p affects the temporal decay rate of soot temperature (Fig. 6b), since the temperature decay rate for larger particles is slower due a smaller surface area-to-volume ratio. In fact, the temporal decay rate of soot particle temperature, $d\ln(T - T_g)/dt$, is inversely proportional to d_p as shown in Eq. (12).

The effect of uncertainty in N_p on the calculated soot particle temperature is shown in Fig. 7 for three different values of N_p, 25, 50, and 100, while keeping other parameters constant and $E(m) = 0.366$ and $\alpha = 0.26$. Results shown in Fig. 7 demonstrate that N_p has almost no effect on the peak temperature and has only a slight effect on the slope of the temporal decay rate

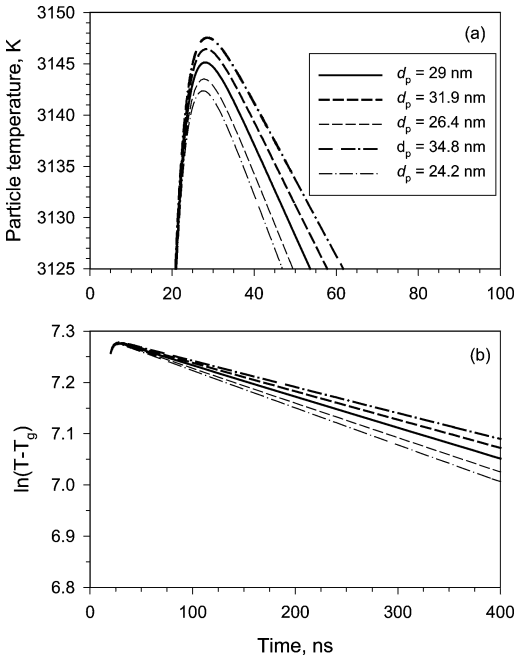

Fig. 6. Effects of the primary soot particle size on the calculated peak soot particle temperature and temporal decay rate at a uniform laser profile with a fluence of 0.9 mJ/mm^2, $\alpha = 0.26$, $E(m) = 0.366$, $N_p = 42$, and the pre factor and exponent in Eq. (5) from Brasil et al. [31].

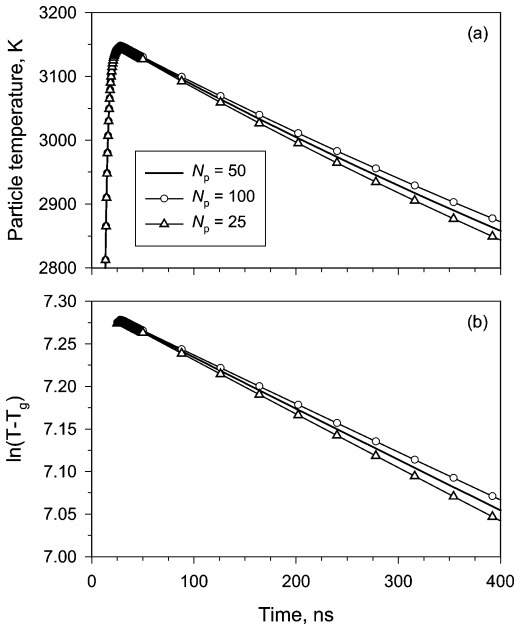

Fig. 7. Effects of the mean aggregate size on the calculated peak soot particle temperature and temporal decay rate at a uniform laser profile with a fluence of 0.9 mJ/mm^2, $\alpha = 0.26$, $E(m) = 0.366$, $d_p = 29$ nm, and the pre factor and exponent in Eq. (5) from Brasil et al. [31].

of soot particle temperature, only about 5% difference from that of $N_p = 50$ for both $N_p = 25$ and $N_p = 100$.

In summary, the numerical results indicate that $E(m)$ affects the peak soot temperature only and α affects the temporal decay rate only. These results are consistent with the theoretical analysis given in Eqs. (11) and (12).

4.2. Determination of $E(m)$ and α using the experimental particle temperature

The experimental soot particle effective temperature was derived using Eq. (2) together with two different assumptions for the wavelength dependence of $E(m)$: (i) $E(m)$ varies linearly with wavelength based on the experimental results of Krishnan et al. [22] and (ii) $E(m)$ is independent of wavelength as suggested by Snelling et al. [26]. The experimentally derived soot temperature history at a laser pulse energy of 2 mJ and assuming linear relation between $E(m)$ and λ is compared with numerically calculated ones in Fig. 8. Under these conditions, the derived values of $E(m)$ at 1064 nm and α are 0.42 and 0.37, respectively, based on the experimental peak temperature and temporal decay rate using Eqs. (11) and (12). Numerical results were obtained using three pairs of $E(m)$ and α: the derived values, $E(m) = 0.42$

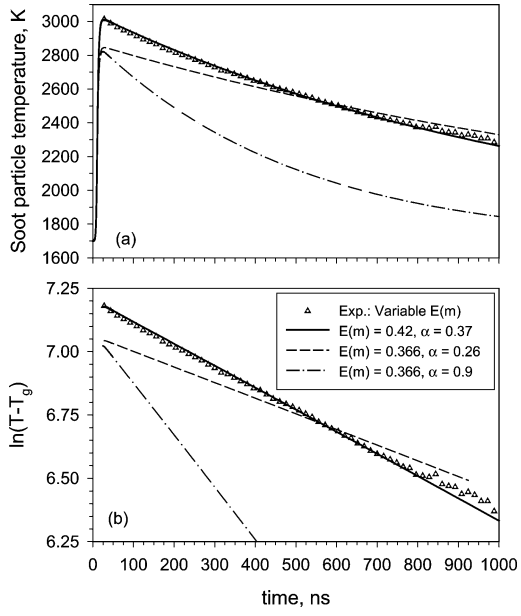

Fig. 8. Comparison of the experimental and numerical effective soot particle temperatures at the laser pulse energy of 2 mJ. The experimental soot particle temperature was determined assuming a linear variation of $E(m)$ with wavelength. The numerical particle temperatures are calculated for different values of $E(m)$ and α, $d_p = 29$ nm, $N_p = 42$, and using the pre factor and exponent of Brasil et al. [31].

and $\alpha = 0.37$, and two pairs from literature, $E(m) = 0.366$, $\alpha = 0.26$ and $E(m) = 0.366$, $\alpha = 0.9$. The derived $E(m)$ is about 15% higher than that suggested by Krishnan et al. [22] at 1064 nm. The numerical soot temperature history based on the derived $E(m)$ and α is indeed in very good agreement with the experimental one for both the peak temperature (Fig. 8a) and the temporal decay rate (Fig. 8b), as expected. On the other hand, the numerical soot temperature histories based on $E(m)$ and α from the literature are in significant discrepancy with the experimental one, indicating that the typical values of $E(m)$ and α commonly used in the LII community are in substantial error.

The experimentally derived soot temperature history at a laser pulse energy of 2 mJ and assuming constant $E(m)$ in the visible and near infrared is compared with numerically calculated ones in Fig. 9. When constant $E(m)$ is assumed, the experimentally derived peak temperature is about 80 K lower than that based on a linear $E(m) \sim \lambda$ relation shown in Fig. 8. As a result, $E(m)$ at 1064 nm calculated using Eq. (11) and the experimental peak temperature shown in Fig. 9a is about 0.395, which is still about 8% higher than that obtained by Krishnan et al. [22]. Based on our TS/TEM-determined mean particle diameter $d_p = 29$ nm, the accommodation coefficient α calculated using Eq. (12) along with the experimental decay rate shown in Fig. 9b is also 0.37, which is also expected.

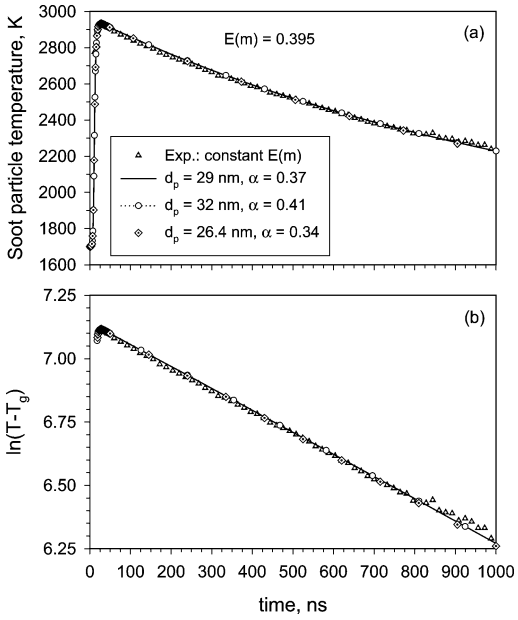

Fig. 9. Comparison of the experimental and numerical effective soot particle temperatures at the laser pulse energy of 2 mJ. The experimental soot particle temperature was determined assuming a wavelength-independent $E(m)$. The numerical particle temperatures are calculated for different values of d_p and α, $N_p = 42$, $E(m) = 0.395$, and using the pre factor and exponent of Brasil et al. [31].

For a *known* soot temperature temporal decay rate, such as obtained experimentally using the three-color optical pyrometer here, Eq. (12) indicates that the derived value of α is proportional to the primary soot particle size d_p. Therefore, if a 10% error is assumed for the determined value of 29 nm for d_p, the derived α would depart from 0.37 also by 10%, in the same direction in order to keep α/d_p constant based on Eq. (12). The results based on a 10% perturbation for both d_p and α are also shown in Fig. 9. These results are almost identical to those based on $d_p = 29$ nm and $\alpha = 0.37$, consistent with the theoretical result given in Eq. (12).

5. Conclusions

A combined numerical and experimental study of laser-heated soot particle temperatures was conducted in a coflow laminar ethylene diffusion flame. The theoretical LII model was improved by taking into account the fractal structure of soot aggregates in the heat conduction submodel. Relatively small uncertainty exists in the experimentally derived particle temperatures due to the uncertainty in the functional dependence of $E(m)$ on wavelength. Both theoretical analysis and numerical results indicate that the peak soot particle temperature near the end of the laser pulse is nearly independent of the primary soot particle size and the aggregate size, which forms the basis to derive the value of $E(m)$ at the laser operation wavelength by making use of the experimentally determined peak soot temperature. Theoretical analysis and numerical results show that the temporal decay rate of soot particle temperature is influenced primarily by the thermal accommodation coefficient and the primary soot particle diameter and secondarily by the aggregate cooling area model and the mean aggregate size.

Using the combined theoretical and experimental approach, the soot absorption function $E(m)$ and the accommodation coefficient α for soot/surrounding gases were derived based on experimentally determined peak soot temperature and temporal temperature decay rate. The uncertainty in the derived value of $E(m)$ is due to the uncertainty in the functional dependence of $E(m)$ on wavelength, which is required to determine the experimental soot particle temperature. The errors in the measured values of the mean primary soot particle size at the location of LII measurement in the laminar ethylene coflow diffusion flame have negligible effects on the value of the de-

rived $E(m)$. The error in the measured value of the primary soot particle size passes directly to the derived thermal accommodation coefficient. Considering uncertainties in the mean aggregate size, the primary soot particle diameter, and aggregate cooling area submodel, the uncertainty associated with the derived value of the thermal accommodation coefficient is likely to be within 15%. Assuming wavelength independence of $E(m)$ and linear variation of $E(m)$ with wavelength, the derived values of the soot absorption function at 1064 nm are respectively 0.395 and 0.42. The thermal accommodation coefficient of soot/surrounding gases was found to be 0.37.

This study explored a new methodology of deriving the values of the soot absorption function and the thermal accommodation coefficient using low-fluence laser-induced incandescence. The novel method presented in this study can be used to determine values of $E(m)$ and α under other conditions. Work is under way to determine the value of $E(m)$ at 532 nm and other wavelengths, which provides new evidence on how $E(m)$ varies with wavelength in the visible and near infrared.

Acknowledgments

The authors acknowledge a large debt of gratitude to Professor Constantine M. Megaridis of the University of Illinois at Chicago, who generously provided advice and material assistance in implementing the soot thermophoretic sampling system. The authors gratefully acknowledge the help of Mr. Kevin Thomson and Dr. Kuo Tian, who performed the TEM analysis, and Mr. Daniel Clavel and Mr. Robert Sawchuk, who assisted with the LII experiments.

References

[1] R.J. Santoro, H.G. Semerjian, R.A. Dobbins, Combust. Flame 51 (1983) 203.
[2] R.A. Dobbins, C.M. Megaridis, Langmuir 3 (1987) 254.
[3] B. Quay, T.-W. Lee, T. Ni, R.J. Santoro, Combust. Flame 97 (1994) 384.
[4] R.L. Vander Wal, K.J. Weiland, Appl. Phys. B 59 (1994) 445.
[5] S. Will, S. Schraml, A. Leipertz, Opt. Lett. 20 (1995) 2342.
[6] C.R. Shaddix, K.C. Smyth, Combust. Flame 107 (1996) 418.
[7] B. Mewes, J.M. Seitzman, Appl. Opt. 36 (1997) 709.
[8] S. Schraml, S. Dankers, K. Bader, S. Will, A. Leipertz, Combust. Flame 120 (2000) 439.
[9] D.R. Snelling, G.J. Smallwood, I.G. Campbell, J.E. Medlock, Ö.L. Gülder, in: AGARD 90th Symposium of the Propulsion and Energetics Panel on Advanced Non-intrusive Instrumentation for Propulsion Engines Brussels, Belgium, 1997.
[10] A.B. Ayling, I.W. Smith, Combust. Flame 18 (1972) 173.
[11] K.L. Cashdollar, Appl. Opt. 18 (1979) 2595.
[12] Y.A. Levendis, K.R. Estrada, H.C. Hottel, Rev. Sci. Instrum. 63 (1992) 3608.
[13] T. Panagiotou, Y. Levendis, M. Delichatsios, Combust. Flame 104 (1996) 272.
[14] Y.R. Sivathanu, J.P. Gore, J. Dolinar, Combust. Sci. Technol. 76 (1991) 45.
[15] A.C. Eckbreth, J. Appl. Phys. 48 (1977) 4473.
[16] D.R. Snelling, G.J. Smallwood, R.A. Sawchuk, W.S. Neill, D. Gareau, D. Clavel, W.L. Chippior, F. Liu, Ö. Gülder, SAE Paper 2000-01-1994, 2000.
[17] C.J. Dasch, Appl. Opt. 23 (1984) 2209.
[18] D.L. Hofeldt, SAE Paper 930079, 1993.
[19] L.A. Melton, Appl. Opt. 23 (1984) 2201.
[20] D.R. Snelling, F. Liu, G.J. Smallwood, Ö.L. Gülder, in: NHTC2000-12132, Proceedings of NHTC '00, 34th National Heat Transfer Conference, Pittsburgh, PA, 2000.
[21] G.J. Smallwood, D.R. Snelling, F. Liu, Ö.L. Gülder, J. Heat Transfer 123 (2001) 814.
[22] S.S. Krishnan, K.-C. Lin, G.M. Faeth, J. Heat Transfer 123 (2001) 331.
[23] D.R. Snelling, K.A. Thomson, G.J. Smallwood, Ö.L. Gülder, Appl. Opt. 38 (1999) 2478.
[24] Ö.L. Gülder, D.R. Snelling, R.A. Sawchuk, Proc. Combust. Inst. 26 (1996) 2351.
[25] Ü.Ö. Köylü, C.S. McEnally, D.E. Rosner, L.D. Pfefferle, Combust. Flame 110 (1997) 494.
[26] D.R. Snelling, K.A. Thomson, G.J. Smallwood, Ö.L. Gülder, E.J. Weckman, R.A. Fraser, AIAA J. 40 (2002) 1789.
[27] C.M. Megaridis, R.A. Dobbins, Combust. Sci. Technol. 71 (1990) 95.
[28] G.M. Faeth, Ü.Ö. Köylü, Combust. Sci. Technol. 108 (1995) 207.
[29] S. Chapman, T.G. Cowling, The Mathematical Theory of Non-uniform Gases, 3rd edition, Cambridge Univ. Press, Cambridge, UK, 1970, p. 249.
[30] B.J. McCoy, C.Y. Cha, Chem. Eng. Sci. 29 (1974) 381.
[31] A.M. Brasil, T.L. Farias, M.G. Carvalho, J. Aerosol Sci. 30 (1999) 1379.
[32] Ü.Ö. Köylü, G.M. Faeth, T.L. Farias, M.G. Carvalho, Combust. Flame 100 (1995) 621.
[33] A.V. Filippov, M. Zurita, D.E. Rosner, J. Colloid Interface Sci. 229 (2000) 261.
[34] G.J. Smallwood, D. Clavel, D. Gareau, R.A. Sawchuk, D.R. Snelling, P.O. Witze, B. Axelsson, W.D. Bachalo, Ö.L. Gülder, SAE Paper 2002-01-2715 (2002).
[35] F. Liu, H. Guo, G.J. Smallwood, Ö.L. Gülder, J. Quant. Spectrosc. Radiat. Transfer 73 (2002) 409.
[36] W.H. Dalzell, A.F. Sarofim, J. Heat Transfer 91 (1969) 100.